

VeREFINE: Integrating Object Pose Verification with Iterative Physics-guided Refinement

Dominik Bauer, Timothy Patten and Markus Vincze

Abstract—Precise object pose estimation for robotics applications and augmented reality relies on final refinement and verification steps. However, interactions between objects and interactions with the supporting structures in the observed scene are typically not considered. In this work, we propose to integrate scene-level hypotheses verification with object-level object pose refinement guided by physics simulation. This allows the physical plausibility of individual object pose estimates and the stability of the estimated scene to be considered in a unified search-based optimization. The proposed method is able to adapt to scenes of multiple objects and efficiently focuses on refining the most promising object poses in multi-hypotheses scenarios. We call this integrated approach *VeREFINE* and evaluate it on two datasets with varying scene complexity. The generality of the approach is shown by using two different pose estimators and two different baseline refiners. Results show improvements over all baselines and on all datasets with the inclusion of our proposed *VeREFINE* approach.

I. INTRODUCTION

Precise and reliable object pose estimates allow robotic systems to successfully grasp objects and to avoid collisions during their movements. The precision of many state-of-the-art object pose estimation methods [1], [2], [3] depends on an additional refinement step. The reliability of the estimates is ensured through a hypotheses-verification step that is tasked with rejecting false estimates and selecting the final object pose estimates among the hypotheses [4], [2].

However, by treating object pose refinement and hypotheses verification as separate steps, the refinement cannot benefit from the scene-level information gathered in the verification process. In turn, verification only decides which hypotheses to include in the solution and does not influence the object-level refinement. Furthermore, errors such as object intersections or physically-unstable initial pose estimates are not dealt with by verification. They require physics to be considered during hypotheses creation.

Recent approaches combine object pose verification [5] or shape estimation [6] with physics simulation. However, they either treat physics and object pose refinement separately [5] or fully rely on physics for refinement [6]. By considering all combinations of hypotheses, the verification part of these methods is computationally expensive and results in frame times of up to 30s [5]. Krull et al. [7] propose to integrate object pose refinement and verification in a reinforcement-learned framework to efficiently allocate a given refinement

This work is partially funded by the TU Wien Doctoral College TrustRobots and the Austrian Science Foundation (FWF) under grant agreement No. I3968-N30 HEAP and No. I3969-N30 InDex.

The authors are with the Automation and Control Institute, TU Wien, 1040 Vienna, Austria {bauer,patten,vincze}@acin.tuwien.ac.at.

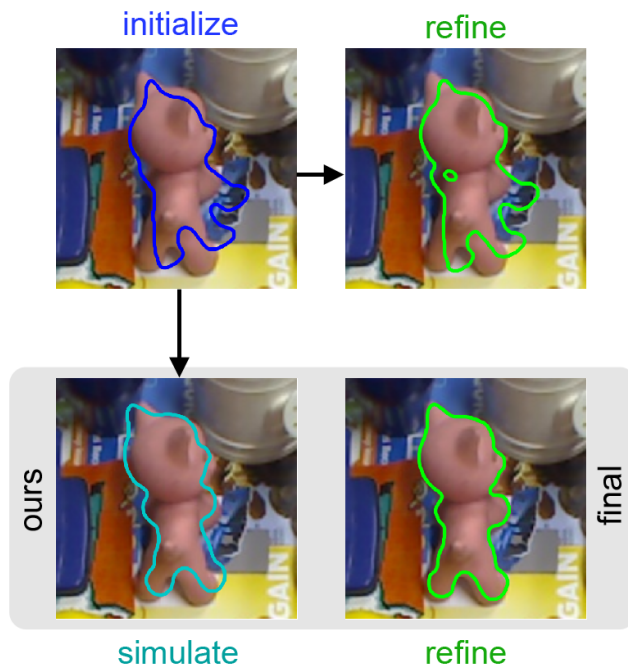


Fig. 1: The proposed *VeREFINE* approach (bottom) merging physics simulation and refinement to recover from poor pose estimates vs. the refinement iteration of the baseline [3].

budget. However, the method does not consider physical plausibility of the pose estimates and the authors report a frame time of up to 34s.

We propose to integrate hypotheses verification and an iterative physics-guided refinement procedure into a unified search-based method called *VeREFINE* (scene-level *Verification* with nested object-level *Refinement*) to overcome the limitations of previous methods (see Figure 1). For Scene-level *Verification* (SV), we propose to find stable object configurations to reduce the search space using physics simulation. The set of object pose estimates that best fit the observation is selected by rendering-based verification. For Object-level *Verification* (OV), we propose Physics-guided Iterative Refinement (PhysIR) to efficiently spend a given number of iterations using a Multi-armed Bandit (MAB) policy. The refinement is provided with the scene-level object configurations for use in simulation. The SV uses the best estimate per object that is found by the OV. Through this integration, both parts support each other. This results in higher performance than treating these steps in isolation. In summary, the contribution is the

- integration of object pose refinement, refinement budget allocation, and hypotheses verification into a unified search-based optimization,
- physics-guided iterative refinement with rendering-based object-level verification,
- exploitation of a fixed refinement budget, and
- ensuring physical stability by scene-level verification.

The proposed approach is evaluated on the LINEMOD and YCB-VIDEO datasets. Our method boosts the performance of existing state-of-the-art methods for iterative refinement by dynamically adapting to multiple objects and multiple hypotheses. With a frame time of 0.5s on LINEMOD and 5s on the YCB-VIDEO dataset, the proposed method is significantly faster than other verification approaches.

II. RELATED WORK

Gravity, collisions, or full physics simulations relate the observed scene and the observer to the world they inhabit, which creates strong cues for orientation and admissible scene configurations. Fei et al. [8] propose to incorporate gravity as a cue in depth estimation, in what they call *Geo-supervision*. The segmentation method by Jia et al. [9] fits boxes that enclose candidate patches that are combined or split based on their physical stability. A similar reasoning to voxelized scene representations to segment and estimate the shape of objects is applied in [10]. In a robotics context, Furrer et al. [11] show the benefit of using physics simulation for object stacking. They propose a method for determining the target pose of irregular stones such that a structurally stable stack can be built by a robot. Song et al. [6] combine shape estimation with a physics-based verification using Monte Carlo Tree Search (MCTS). The MCTS searches the space of all combinations of given shape hypotheses by determining a stable stack of shapes. Mitash et al. [5] use physics-based verification and MCTS for object pose estimation. This is similar to our work, however, all hypotheses are considered at the scene level, which creates a huge search space. In contrast, we prune implausible combinations and reduce complexity by considering objects at the scene level and capsule their hypotheses in a nested object-level refinement. For each combination, the method in [5] runs Trimmed Iterative Closest Point (ICP) and a physics simulation. Thus, computation is spent on implausible combinations. By running physics simulation once after refinement, the method is more sensitive to the estimation of the supporting plane and the physical properties of the simulated objects. Our proposed solution of interleaving physics and refinement is more robust to these issues.

Previous work on object pose refinement exploits depth, RGB and object segmentation as input modalities. A seminal approach is ICP and its many variants [12], [13], [14]. More recently, deep learning based approaches to the object pose refinement problem have been proposed. RGB-based methods render intermediary object pose estimates and use CNNs to compute a pose update [15], [16]. Instance segmentation

is used to guide the computation of the pose update [17], [18]. The refinement method proposed by Wang et al. [3] requires RGB-D images and instance segmentation as input. The additional depth cues are processed using PointNet [19] and combined with the RGB-based features from a CNN. During iterative refinement, the PointNet features are updated by processing the updated estimate’s point cloud and the following pose update is computed.

Hypotheses verification approaches for object pose estimation show that considering multiple candidate hypotheses per object improves overall estimation performance. Vidal et al. [1] generate a pool of 200 object pose hypotheses using a Point Pair Features (PPF) pipeline, refine each hypothesis using Projective ICP and apply a two-step verification to determine the best estimate. Drost et al. [4] replace separate pose refinement with a clustering-based verification stage. Hypotheses in the top-scoring cluster are averaged to increase the accuracy of final pose estimate. SegICP [20] generates a pool of hypotheses by rendering the initial candidate pose at different camera angles. The resulting point clouds are compared to the observed point cloud and the highest scoring estimate is selected. Similarly, Xiang et al. [2] perturb an initial pose estimate to generate a set of hypotheses for better coverage of the solution space. All hypotheses are refined before scoring and selection. In contrast, Wang et al. [3] propose to estimate a pose confidence score jointly with per-pixel object pose estimates. The highest scoring estimate is selected and refined to compute the final estimate. Krull et al. [7] train a CNN to predict two different hypotheses scores for use during refinement and for the selection of the final estimate. They concatenate a feature vector containing the number of refinement iterations and distance to other hypotheses to the first fully-connected layer of their scoring network. On the scene level, Aldoma et al. [21] propose a scoring function that considers geometrical cues, clutter and conflicting hypotheses for multiple objects. An alternative approach is to exhaustively search the combination of hypotheses that reduces the discrepancy of the observed depth image and a depth rendering of the resulting candidate scene [22]. For more efficient evaluation of the search space, [23] consider equivalent combinations of hypotheses to reduce the search tree to a directed acyclic graph and explore using MCTS. Physics simulation is incorporated in MCTS to additionally consider the supporting relations between objects in [5], [24].

In this work, we verify the physical plausibility and scene fit of object hypotheses at the scene-level while refining and verifying individual pose hypotheses at the object-level. Thereby, we reduce the search space as compared to other search-based methods, are able to more efficiently allocate refinement steps to individual pose hypotheses and improve the quality of pose estimates by integrating refinement with physics simulation.

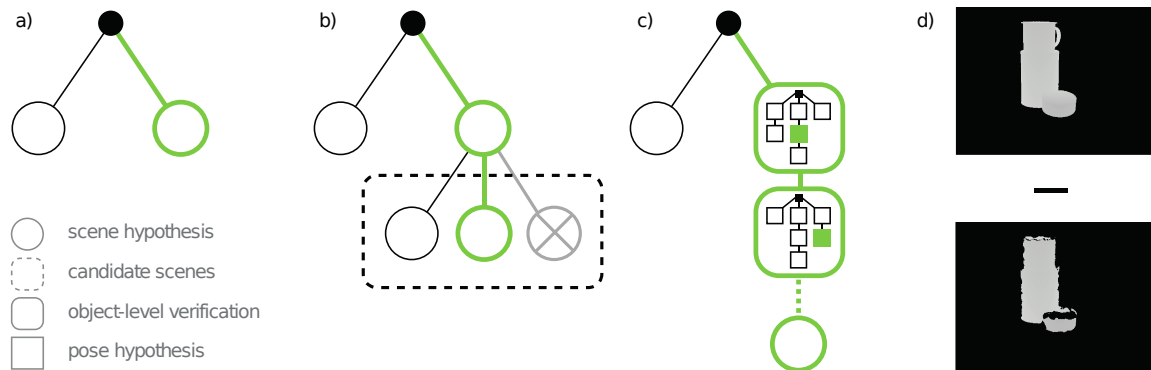


Fig. 2: Overview of one iteration of VeREFINE, illustrating the four steps of SV. The current best candidate scene is selected (a) and a new physically stable candidate scene is created by adding an object to the best candidate (b). Unstable candidates are pruned (light gray in b). The rollout phase (c) triggers the nested OV to find the best pose hypothesis for each object. A final scene is simulated by adding the missing objects in a random pose (dashed in c). Finally, the reward for the final scene is computed based on depth-discrepancy between the rendered scene (top d) and the observation (bottom d). The reward is backpropagated along the descent path.

III. INTEGRATING HYPOTHESES VERIFICATION WITH ITERATIVE PHYSICS-GUIDED REFINEMENT

Precisely and reliably estimating the pose of each object in complex, cluttered scenes yields several problems. On the scene level, every object requires stable support and must not intersect other objects. Also, parts of objects are hidden through occlusion. On the object level, the pose of an object must obey the laws of physics and plausibly explain the related visual observation. Previous work tackles subsets of these problems by different combinations of object pose refinement, physical simulation and hypotheses verification. Considering all mentioned problems at once, however, requires tight integration of the three approaches. To this end, we propose the approach outlined in Figure 2.

Scene-level problems are addressed by iteratively building candidate scenes, which are represented as nodes in a search tree. Objects are added to the candidate scenes based on physical stability and a rendering-based verification score. The resulting SV is discussed in Section III-A.

Physical plausibility of hypotheses on the object-level is enforced by integrating physics simulation with iterative object pose refinement (illustrated by the tree nodes in Figure 2c). Time spent on refinement is limited by a fixed budget, dynamically allocated based on the fitness score of the intermediary estimates. Section III-B discusses the OV in more detail.

The integration of SV and OV allows both parts to share information. For example, on the scene level, precise pose estimates per object are required to create stable candidate scenes. On the object level, the simulation of candidate hypotheses requires a stable estimate of the scene. The details of the proposed integration are discussed in Section III-C.

A. Scene-level Verification

The task of SV is to determine stable candidate scenes and to select the candidate that best explains the observed scene. By iteratively adding objects to candidates, SV grows

a search tree in which each node represents a stable scene. We employ two strategies to guide the growth of this search tree. First, to contain the size of the search space, only objects that are in contact with the candidate scene are considered. This also guarantees that all candidate scenes are physically stable. Second, to reach an optimal candidate scene in limited time, a tree search policy selects the candidate that should be expanded next.

1) *Finding Isolated Object Clusters*: The order in which objects are placed in a scene is important. Simulating an object without its support being present in the scene will yield incorrect results. Hence, not only all subsets of objects but also all orders of placing them in the scene have to be considered. This leads to an exponential growth of the search space with growing number of interacting objects. In SV, the growth is limited by clustering objects according to potential interactions and considering these clusters in isolation.

In contrast to the rendering-based clustering of object pose hypotheses proposed by Mitash et al. [5], we utilize the physics simulation’s collision detection. The collision-based clustering first instantiates all objects in their initial pose estimate. The contact points between each object and all others are accumulated into an adjacency matrix that encodes interacting objects. Finally, separate clusters are determined by applying the Cuthill-McKee algorithm [25] to the adjacency matrix. This reorders the adjacency matrix into a block diagonal form where blocks correspond to clusters. Each cluster is treated in isolation to reduce the search space. In these clusters not all objects influence one another but rather only their adjacent objects. By only considering potentially interacting objects for growing the search tree, the search space is further reduced.

2) *Search-based Verification*: To contain the time spent per frame, the goal is to find an optimal candidate scene within a fixed number of search iterations. The regret of exploring suboptimal candidates instead of the optimal ones should be minimized. This is achieved by guiding the search

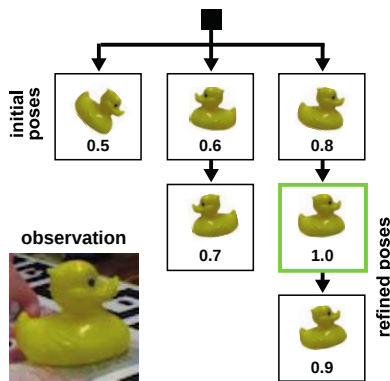


Fig. 3: Illustration of OV. The Budget Allocation Bandit (BAB) allocates a budget of three refinements and selects the best scoring pose estimate (green).

using the UCB1 policy. Applying the UCB policy to tree search is commonly referred to as UCT or simply MCTS. MCTS consists of four phases that are repeated until the fixed number of iterations is spent. In SV the phases are implemented as follows: In the first phase, starting from the root that represents the ground plane, UCB1 is applied to select the optimal candidate scene until a leaf node is reached. This is illustrated in Figure 2a. The second phase, shown in Figure 2b, expands the search tree by adding one of the potentially interacting objects and creates a new child node that represents the new candidate scene. The third phase, the rollout, samples the reward that can be expected from selecting this candidate scene in consecutive iterations. This process is illustrated in Figure 2c. We apply OV to all objects in the candidate scene in the order they are placed. This way, the objects in the candidate scene are represented by their most plausible hypothesis. To simulate a final candidate scene, missing objects are added using a random pose hypothesis. Finally, the new candidate’s reward is backpropagated to all nodes along the descent path and a new iteration is started from the root node. We define the reward based on the depth-discrepancy of the candidate and the observed scene based on the definition in [26]. Figure 2d gives an example for the used depth images. Note that, for a scene with a single object, this is equivalent to just applying OV. The proposed approach thus dynamically adapts to this variation in scene complexity.

B. Object-level Verification

The goal of OV is to decide which hypotheses to refine, how often to make refinements, and finally, decide on the best resulting hypothesis. The fixed amount of refinements that should be spent per object will be referred to as *refinement budget*. We propose to model the allocation of the refinement budget as a MAB. In addition, we present a physics-guided extension to iterative refinement methods, called PhysIR, that progresses the refinement towards physically plausible object poses.

1) *Budget Allocation Bandit*: An optimal refinement-budget allocation must trade-off exploration of different hy-

potheses and exploitation of promising hypotheses. A well-studied approach to tackle the explore-exploit dilemma are policies for playing MABs. The idea is that playing an arm yields a reward that is sampled from an unknown distribution. The goal of the policy is to minimize the regret due to plays of sub-optimal arms in a series of plays. Analogously, we propose to minimize the regret due to refining a sub-optimal hypothesis. Each estimate in an object’s estimate pool is modeled as an arm of a bandit. Playing an arm runs one iteration of PhysIR and returns the new estimate’s verification score as a reward. The verification score is computed by determining the discrepancy between the observed depth and the rendered depth image as defined in [26]. In each iteration, the policy selects the most promising estimate to refine and updates its statistics for the next iteration. This procedure is repeated until the refinement budget is spent. Finally, the hypothesis with the best verification score is returned. We call this approach BAB. It is outlined in Figure 3.

2) *Iterative Physics-guided Refinement*: Iterative refinement approaches generally consist of two steps [27]. First, features of the current estimate and the observation are associated. Second, an updated estimate is computed to minimize the distance between associated points. These steps are repeated until a stopping criterion is satisfied. However, iterative refinement can become stuck in local minima or even diverge from the true object pose. This translates to tilted, floating and intersecting object pose estimates.

These physically implausibilities are resolved by applying physics simulation. In addition, the physics simulation progresses the iterative refinement procedure towards the true object pose. Our proposed method, PhysIR, extends other iterative refinement methods to boost their performance. We add a physics simulation step before each iterative refinement step to create better initial estimates for each iteration. Figure 1 illustrates the procedure for one refinement iteration – while the baseline refinement cannot cope with the imprecise initialization, the proposed approach improves the initial estimate using physics simulation before feeding it to the refinement step. There are cases where simply simulating the estimate may move too far from the observation. For example, a bad initialization may lead to the object to topple over in simulation, which will invalidate all associations with the observation. This is contained by only updating the estimate’s rotation around the object center with the simulated rotation. Thus, the estimated pose remains centered around the same point in space.

C. Integration of Scene-level and Object-level

For the integration, SV and OV need to share information about the candidate scene as well as the hypotheses of the candidate objects. Thereby, the tight integration of both parts allows for each subtask to benefit from the information gathered on both the scene and the object level.

The reasoning on physical stability at the scene level builds on the best refined hypotheses from the object level. In turn, the object level uses the current candidate scene from the scene level as the environment for simulation and refinement.

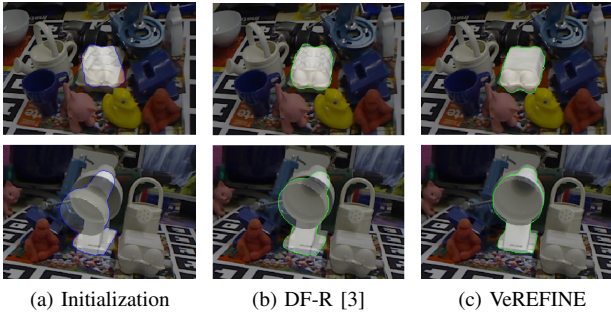


Fig. 4: Qualitative examples on LINEMOD.

As a result, the integration addresses the problem of physical plausibility on both levels in a coherent manner.

In summary, the verification of individual hypotheses at object level help to guide the scene-level search towards more promising regions. The verification at scene level helps to avoid spending time on refining implausible scene configuration at the object level.

IV. RESULTS

This section presents the evaluation of our proposed approach on the LINEMOD and YCB-VIDEO datasets. Improvement over state of the art is shown by comparing to PoseCNN (PC)+DeepIM (DIM) [18] and DenseFusion (DF) [3]. The impact of the individual parts PhysIR, OV and SV is evaluated in an ablation study on YCB-VIDEO. Experiments with varying number of simulation steps and refinement iterations illustrate the need for a balance between physics simulation and iterative refinement. Finally, the is BAB compared with other budget allocation approaches.

Datasets: The LINEMOD dataset [28] is used to evaluate the performance in the single-object setting. The same test set as in prior work [18], [3] is used, i.e., scenes 3 and 7 are excluded from the test set. YCB-VIDEO [2] is used in the multi-object setting. The reduced test set defined in [29] is used. It features test images with higher annotation quality [29] than the full test set used in [18], [3].

Metrics: For evaluation on LINEMOD, we use the AD , n° , $n\text{ cm}$ and $PROJ$ metrics as defined in [18]. The AD metric [28] uses the ADI metric for symmetric objects and the ADD metric for non-symmetric objects. For accepted estimates, the average distance between points in the estimated pose and points in the ground-truth pose may not exceed $x \cdot d$ where d is the diameter of the object. The n° , $n\text{ cm}$ metric [30] accepts the estimated pose if it does not differ from the ground-truth pose by more than a n° rotation and a $n\text{ cm}$ translation. The $PROJ$ metric [31] accepts estimates if the average distance between the 2D projection of points in the estimated pose and points in the ground-truth pose do not exceed n pixels. The criteria of the n° , $n\text{ cm}$ and $PROJ$ metrics for symmetric objects must only be fulfilled for one of the symmetric ground-truth poses.

For the evaluation on YCB-VIDEO, the area under the accuracy curve (AUC) is determined by computing the recall for ADI thresholds between 0 and 10cm as defined in

TABLE I: Comparison with baseline on LINEMOD.

Metric	PCNN+DIM	+VeREFINE	DF+DF-R	+VeREFINE
$AD_{0.05d}$	69.2	70.5 (+1.3)	84.7	92.4 (+7.7)
$AD_{0.10d}$	88.6	89.2 (+0.6)	94.3	97.3 (+3.0)
$2^\circ, 2\text{cm}$	39.0	42.5 (+3.5)	27.1	41.4 (+14.3)
$5^\circ, 5\text{cm}$	85.2	88.5 (+3.3)	61.3	82.6 (+21.3)
$PROJ_{2px}$	75.6	76.8 (+1.2)	42.2	54.6 (+12.4)
$PROJ_{5px}$	97.5	98.0 (+0.5)	74.9	90.2 (+15.3)

TABLE II: Comparison with baseline on YCB-VIDEO.

Metric	DF+DF-R	+VeREFINE
MSPD	54.6	57.2 (+2.6)
MSSD	70.7	73.0 (+2.3)
MVSD	51.5	52.7 (+1.2)
AR	58.9	61.0 (+2.1)
$ADI_{1\text{cm}}$	89.0	91.9 (+2.9)
$ADI_{2\text{cm}}$	96.7	96.4 (-0.3)
$AUC_{2\text{cm}}$	76.0	79.5 (+3.5)
$AUC_{10\text{cm}}$	93.2	93.7 (+0.5)

[2]. In addition, the evaluation procedure defined for the BOP 2019 challenge [29] is used as it thoroughly considers different aspects of object pose estimation quality at different precision levels. Scores are reported for all three metrics (MSPD, MSSD, MVSD) as well as the overall performance score (AR) that averages the scores of the metrics over all thresholds as defined in [29].

Baselines: Precomputed detections and segmentation masks are provided by [2] for LINEMOD and YCB-VIDEO. For PC we use the precomputed pose estimates from LINEMOD and YCB-VIDEO. For DF, we generated a pool of object pose estimates using the provided code and weights. The hypotheses pool consists of the highest confidence per-pixel estimate and four uniformly random sampled estimates.

The generality of our approach is shown by applying it to two baseline iterative refinement approaches, namely DIM and the refinement network used in DF (referred to as *DF-Refine* (DF-R) to avoid confusion with the pose estimation method of same name). The provided weights from [18] are used for evaluation of DIM on LINEMOD and the weights from [3] are used for evaluating DF-Refine on LINEMOD and YCB-VIDEO. DIM is extended by performing physics simulation before the rendering of the estimate. The extension to DF uses the estimate of the physics simulation to transform the input point cloud. We apply four iterations of DIM and two iterations of DF-R per hypothesis. The overall refinement budget per frame is $n_o \cdot n_h \cdot n_i$, where n_o is the *number of objects* in the scene, n_h is the *number of hypotheses* per object and n_i is the *number of iterations* per hypothesis. PyBullet is used as the physics simulation framework.

A. Comparison with State of the Art

The proposed approach is compared with two state-of-the-art methods. PCNN+DIM refines a single hypothesis for a single object in the LINEMOD dataset. Therefore, *VeREFINE* is only influenced by applying PhysIR to DIM. DF+DF-R computes per-pixel pose estimates along with

TABLE III: Ablation study of the proposed methods on YCB-VIDEO.

Metric	DF+DF-R	PhysIR	PhysIR+SV	PhysIR+OV	VeREFINE
ADI_{1cm}	89.0	89.1	91.5	91.8	91.9
AUC_{2cm}	76.0	76.5	78.7	79.4	79.5
t_{frame}	0.02s	0.15s	0.91s	1.85s	5.33s

a confidence score for each estimate. The highest scoring estimate is selected and refined using two iterations of DF-R. For *VeREFINE*, we apply OV to a pool of five per-pixel estimates. As YCB-VIDEO contains multiple objects per scene, the results of *VeREFINE* also reflect the impact of the SV.

As shown in Table I and II, VeREFINE is able to boost the performance of both baselines on both datasets. The most significant improvement can be observed for the extension to DF on the LINEMOD dataset with an improvement of 21.3% on the $5^\circ, 5cm$ metric. The performance of DF-R degrades when the refinement procedure jumps between supposedly symmetric poses, for example shown in Figure 4b, with the eggbox upside-down and upright. The resulting error in terms of rotation violates the degree limit of the metric. This behavior can be observed in Figure 5 (bottom) and is due to DF-R minimizing the distance to the closest surface points, unaware that upside down is no valid symmetric pose for, e.g., the eggbox. Through object-level verification, VeREFINE is able to select the correct estimate for symmetric objects. On the *PROJ* metric, there is little room for depth-discrepancy verification to improve upon the performance of rendering-based refinement of DIM. Still, a significant improvement can be observed for the more restrictive thresholds of all three metrics. As with DF-R, largest improvement can be observed for the $n^\circ, n cm$ metric.

B. Impact of the Individual Methods

The impact of the individual parts of the presented method is assessed by comparing results using the baseline DF-R to additionally using PhysIR, SV with PhysIR, OV with PhysIR and the full VeREFINE approach. Using SV only with PhysIR highlights the impact of considering multiple objects while using only OV with PhysIR shows the improvement due to considering multiple hypotheses. As shown in Table III, adding OV to PhysIR results in the largest improvement of 2.9% on the AUC_{2cm} metric. While PhysIR considers a single hypothesis, a hypotheses pool of five pose estimates is used in OV. The combination with SV in the full VeREFINE approach results in a further slight improvement.

C. Balance of Simulation and Refinement Iterations

Figure 5 (top) illustrates the impact of the number of physics-simulation steps on the frametime and the performance in terms of AR. Note that 0 simulation steps is equal to the baseline DF-R. A single step progresses the simulation by 5ms. For YCB-VIDEO, using ten steps maximizes performance while minimizing frametime. For LINEMOD, 100 steps are determined to be optimal with a frametime of 64ms for a single hypothesis.

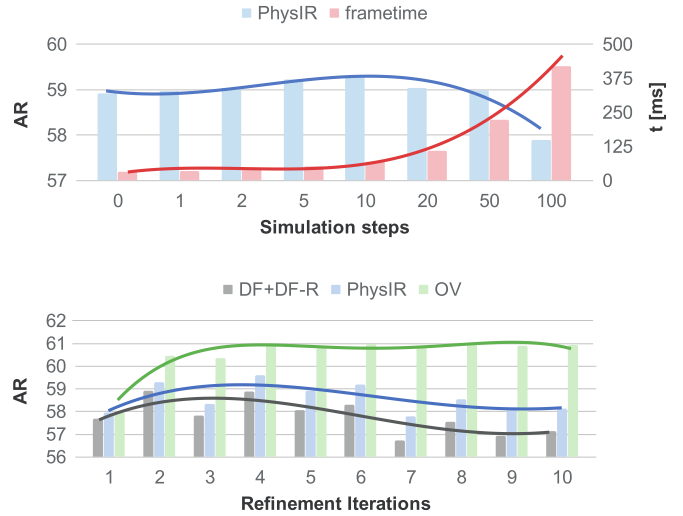


Fig. 5: Comparison of the simulation steps (top) and refinement iterations (bottom) on a subset of YCB-VIDEO for one hypothesis per object. Raw data (bars) and regression (lines).

TABLE IV: Comparison of OV approaches on YCB-VIDEO.

Metric	n_h	equal	exploit	BAB	t_{frame}
AR	2	59.3	59.5	60.9	0.61s

The impact of the number of refinement iterations per object is shown in Figure 5 (bottom). The comparison of the baseline DF-R with PhysIR supports the observation that physics simulation helps to keep iterative refinement from diverging and progressing it towards the true object pose. Note that DF-R is trained to use two iterations.

D. Choice of Budget Allocation Policy

We compare the proposed BAB to two other approaches for dealing with multiple estimates. *Equal* is inspired by the approach of Xiang et al. [2] that spends the refinement budget equally on all estimates in the pool before selecting the best scoring hypothesis. *Exploit* spends the full refinement budget on the top-ranking estimate, as in [3]. Table IV shows the results for using the UCB1 [32] policy with the BAB. All approaches and policies use DF+DF-R with PhysIR and a refinement budget of $2 \cdot n_h$.

The *equal* approach is limited by the discriminative power of the scoring function. The reduced performance of *exploit*, on the other hand, is due to divergence of the iterative refinement when applying all iterations to a single hypothesis. See Figure 5 (bottom) for an illustration of this behavior. The BAB is able to overcome these limitations by dynamically allocating the refinement budget to the most promising hypotheses. Consequently, when a hypothesis starts to diverge, the remaining budget is used to explore other hypotheses. This results in an improved performance even though the scoring function is inferior to the confidence estimates of DF-R and *exploit*.

V. CONCLUSION

This work presented an approach for the tight integration of scene-level and object-level methods for object pose refinement and verification. The search-based hypotheses verification and the proposed physics-guided extension to iterative refinement benefit from this integration by being able to share useful information. The comparison with state-of-the-art methods shows that our integrated approach creates more precise and more reliable object pose estimates.

The use of physics simulation requires fixed structures on which objects can rest and an estimate for the gravity vector. This work uses 3D plane segmentation to determine a supporting plane and uses the normal to determine the gravity direction. For robotic applications, static objects with non-planar surface in the robot's environment map could be considered as supporting structures. An IMU, as shown in previous work [8], could be used to determine the gravity direction to become robust to tilted or non-planar support.

An open issue for robot systems is the presence of a-priori unknown objects. The presented method is able to deal with unknown supporting objects as long as they can be approximated by a plane parallel to the detected supporting plane. If the interactions between known and unknown objects become more complex, the results of simulation will diverge from the true object pose. Incorporating shape estimation [6], [33] would enable these cases to be considered.

REFERENCES

- [1] J. Vidal, C.-Y. Lin, and R. Martí, "6d pose estimation using an improved method based on point pair features," in *International Conference on Control, Automation and Robotics*, 2018, pp. 405–409.
- [2] Y. Xiang, T. Schmidt, V. Narayanan, and D. Fox, "Posecnn: A convolutional neural network for 6d object pose estimation in cluttered scenes," in *CoRR*, 2017.
- [3] C. Wang, D. Xu, Y. Zhu, R. Martín-Martín, C. Lu, L. Fei-Fei, and S. Savarese, "Densefusion: 6d object pose estimation by iterative dense fusion," in *IEEE Conference on Computer Vision and Pattern Recognition*, 2019.
- [4] B. Drost, M. Ulrich, N. Navab, and S. Ilic, "Model globally, match locally: Efficient and robust 3d object recognition," in *IEEE Conference on Computer Vision and Pattern Recognition*, 2010, pp. 998–1005.
- [5] C. Mitash, A. Boularias, and K. E. Bekris, "Improving 6d pose estimation of objects in clutter via physics-aware monte carlo tree search," in *IEEE International Conference on Robotics and Automation (ICRA)*, 2018, pp. 1–8.
- [6] C. Song and A. Boularias, "Inferring 3d shapes of unknown rigid objects in clutter through inverse physics reasoning," *IEEE Robotics and Automation Letters*, vol. 4, no. 2, pp. 201–208, 2018.
- [7] A. Krull, E. Brachmann, S. Nowozin, F. Michel, J. Shotton, and C. Rother, "Poseagent: Budget-constrained 6d object pose estimation via reinforcement learning," in *IEEE Conference on Computer Vision and Pattern Recognition*, 2017, pp. 6702–6710.
- [8] X. Fei, A. Wong, and S. Soatto, "Geo-supervised visual depth prediction," *IEEE Robotics and Automation Letters*, vol. 4, no. 2, pp. 1661–1668, 2019.
- [9] Z. Jia, A. C. Gallagher, A. Saxena, and T. Chen, "3d reasoning from blocks to stability," *IEEE transactions on pattern analysis and machine intelligence*, vol. 37, no. 5, pp. 905–918, 2014.
- [10] B. Zheng, Y. Zhao, J. Yu, K. Ikeuchi, and S.-C. Zhu, "Scene understanding by reasoning stability and safety," *International Journal of Computer Vision*, vol. 112, no. 2, pp. 221–238, 2015.
- [11] F. Furrer, M. Wermelinger, H. Yoshida, F. Gramazio, M. Kohler, R. Siegwart, and M. Hutter, "Autonomous robotic stone stacking with online next best object target pose planning," in *IEEE International Conference on Robotics and Automation (ICRA)*. IEEE, 2017, pp. 2350–2356.
- [12] P. J. Besl and N. D. McKay, "Method for registration of 3-d shapes," in *Sensor fusion IV: control paradigms and data structures*, vol. 1611. International Society for Optics and Photonics, 1992, pp. 586–606.
- [13] Y. Chen and G. Medioni, "Object modelling by registration of multiple range images," *Image and vision computing*, vol. 10, no. 3, pp. 145–155, 1992.
- [14] S. Rusinkiewicz and M. Levoy, "Efficient variants of the icp algorithm," in *3dim*, vol. 1, 2001, pp. 145–152.
- [15] F. Manhardt, W. Kehl, N. Navab, and F. Tombari, "Deep model-based 6d pose refinement in rgb," in *European Conference on Computer Vision (ECCV)*, 2018, pp. 800–815.
- [16] S. Zakharov, I. Shugurov, and S. Ilic, "Dpod: Dense 6d pose object detector in rgb images," *arXiv preprint arXiv:1902.11020*, 2019.
- [17] M. Rad and V. Lepetit, "Bb8: A scalable, accurate, robust to partial occlusion method for predicting the 3d poses of challenging objects without using depth," in *IEEE International Conference on Computer Vision*, 2017, pp. 3828–3836.
- [18] Y. Li, G. Wang, X. Ji, Y. Xiang, and D. Fox, "Deepim: Deep iterative matching for 6d pose estimation," in *European Conference on Computer Vision (ECCV)*, 2018, pp. 683–698.
- [19] C. R. Qi, H. Su, K. Mo, and L. J. Guibas, "Pointnet: Deep learning on point sets for 3d classification and segmentation," in *IEEE Conference on Computer Vision and Pattern Recognition*, 2017, pp. 652–660.
- [20] J. M. Wong, V. Kee, T. Le, S. Wagner, G.-L. Mariottini, A. Schneider, L. Hamilton, R. Chipalkatty, M. Hebert, D. M. Johnson *et al.*, "Segicp: Integrated deep semantic segmentation and pose estimation," in *IEEE/RSJ International Conference on Intelligent Robots and Systems (IROS)*. IEEE, 2017, pp. 5784–5789.
- [21] A. Aldoma, F. Tombari, L. Di Stefano, and M. Vincze, "A global hypothesis verification framework for 3d object recognition in clutter," *IEEE transactions on pattern analysis and machine intelligence*, vol. 38, no. 7, pp. 1383–1396, 2016.
- [22] V. Narayanan and M. Likhachev, "Perch: Perception via search for multi-object recognition and localization," in *IEEE International Conference on Robotics and Automation (ICRA)*, 2016, pp. 5052–5059.
- [23] D. Bauer, T. Patten, and M. Vincze, "Monte carlo tree search on directed acyclic graphs for object pose verification," in *Computer Vision Systems*, 2019 (accepted).
- [24] —, "6d object pose verification via confidence-based monte carlo tree search and constrained physics simulation," in *OAGM & ARW Joint Workshop*, 2019, pp. 153–158.
- [25] E. Cuthill and J. McKee, "Reducing the bandwidth of sparse symmetric matrices," in *24th national conference*. ACM, 1969, pp. 157–172.
- [26] X. Deng, A. Mousavian, Y. Xiang, F. Xia, T. Bretl, and D. Fox, "Poserbpf: A rao-blackwellized particle filter for 6d object pose tracking," *arXiv preprint arXiv:1905.09304*, 2019.
- [27] F. Pomerleau, F. Colas, and R. Siegwart, "A review of point cloud registration algorithms for mobile robotics," *Foundations and Trends in Robotics*, vol. 4, pp. 1–104, 05 2015.
- [28] S. Hinterstoisser, V. Lepetit, S. Ilic, S. Holzer, G. Bradski, K. Konolige, and N. Navab, "Model based training, detection and pose estimation of texture-less 3d objects in heavily cluttered scenes," in *Asian conference on computer vision*. Springer, 2012, pp. 548–562.
- [29] T. Hodaň, E. Brachmann, B. Drost, F. Michel, M. Sundermeyer, J. Matas, and C. Rother, "BOP: Benchmark for 6D Object Pose Estimation," <https://bop.felk.cvut.cz/challenges/bop-challenge-2019/>, 2019, [Online; accessed 04-September-2019].
- [30] J. Shotton, B. Glocker, C. Zach, S. Izadi, A. Criminisi, and A. Fitzgibbon, "Scene coordinate regression forests for camera relocalization in rgb-d images," in *IEEE Conference on Computer Vision and Pattern Recognition*, 2013, pp. 2930–2937.
- [31] E. Brachmann, F. Michel, A. Krull, M. Ying Yang, S. Gumhold *et al.*, "Uncertainty-driven 6d pose estimation of objects and scenes from a single rgb image," in *IEEE Conference on Computer Vision and Pattern Recognition*, 2016, pp. 3364–3372.
- [32] P. Auer, N. Cesa-Bianchi, and P. Fischer, "Finite-time analysis of the multiarmed bandit problem," *Machine learning*, vol. 47, no. 2-3, pp. 235–256, 2002.
- [33] M. Firman, O. Mac Aodha, S. Julier, and G. J. Brostow, "Structured prediction of unobserved voxels from a single depth image," in *IEEE Conference on Computer Vision and Pattern Recognition*, 2016, pp. 5431–5440.